Journal of Biomolecular NMR, 5 (1995) 383–396
ESCOM

J-Bio NMR 250

Manifestation of intramolecular motions on pico- and nanosecond time scales in ^{1}H-^{15}N NMR relaxation: Analysis of dynamic models of one- and two-helical subunits of bacterioopsin

Konstantine V. Pervushin, Vladislav Yu. Orekhov, Dmitry M. Korzhnev and Alexander S. Arseniev*

Shemyakin and Ovchinnikov Institute of Bioorganic Chemistry, Russian Academy of Sciences, Ul. Miklukho-Maklaya 16/10, Moscow 117871, Russia

Received 8 July 1994
Accepted 26 October 1994

Keywords: Molecular dynamics simulation; Heteronuclear; Micelles; Bacterioopsin; Spatial structure; Helix–helix interaction; Relaxation; Membrane proteins

Summary

The influence of the internal dynamics of two polypeptides comprising transmembrane α-helix A or two α-helices A and B of bacterioopsin on experimentally accessible ^{15}N NMR relaxation rates was investigated by molecular dynamics (MD) simulations, combined with more simple mechanic considerations. 'Model-free' order parameters and correlation times of internal motions [Lipari, G. and Szabo, A. (1982) *J. Am. Chem. Soc.*, **104**, 4546–4559] were calculated for these models. It was found that both peptides exhibit two types of internal motions of the amide bonds, on the pico- and nanosecond time scales, affecting ^{15}N NMR relaxation. The fast fluctuations are local and correspond to the librational motions of the individual N-H vectors in an effective potential of atoms of the surrounding matrix. In contrast, the motions on the nanosecond time scale imply concerted collective vibrations of a large number of atoms and could be represented as bending oscillation of α-helices, strongly overdamped by the ambient solvent. A few other molecular mechanisms of slow internal motion were found, such as local distortions of the α-helices (e.g., α-aneurysm), delocalized distortions of the α-helical backbone, as well as oscillations of the tilt angle between the axes of the α-helices A and B. The results are compared with ^{15}N NMR relaxation data measured for the (1–36)bacterioopsin and (1–71)bacterioopsin polypeptides in chloroform–methanol (1:1) and in SDS micelles [Orekhov, V.Yu., Pervushin, K.V. and Arseniev, A.S. (1994) *Eur. J. Biochem.*, **219**, 887–896].

Introduction

The fast development of NMR techniques in the last years has enabled the experimental characterization of the internal motions of different water-soluble proteins (for a recent review see Wagner, 1993). It was shown that the NMR relaxation of ^{15}N and ^{13}C nuclei can be sensitive to the local fluctuations of atoms on the picosecond time scale, more collective motions of large groups of atoms on time scales ranging from 10 ps to 1 ns or longer, up to the overall rotational correlation times of proteins and conformational exchange on the millisecond time scale. NMR techniques have been developed enabling to distinguish conformational exchange processes from rather faster internal motions and to treat them separately (Szyperski et al., 1993; Barchi et al., 1994; Orekhov et al., 1994a). Whereas the molecular mechanics of fast internal fluctuations of atoms have been extensively characterized by MD simulations and normal-mode analyses (Levy and Karplus, 1979; Swaminathan et al., 1982; Levitt et al., 1985; Bruschweiler et al., 1992), the interpretation of low-frequency vibrations, occurring on intermediate time scales, is still in progress.

To understand the mechanics of the low-frequency internal motions contributing to ^{15}N NMR relaxation, development of a particular molecular model, followed by

*To whom correspondence should be addressed.

Abbreviations: C2, bacterioopsin-(7–63)-peptide; sA, bacterioopsin-(7–32)-peptide; CPMG, Carr–Purcell–Meiboom–Gill; MD, molecular dynamics; rmsd, root-mean-square deviation.

testing it against experimental NMR data, is required. The construction of a model for internal motions is usually based on the mechanical considerations of proteins as an elastic body (for reviews see Persson, 1986; Chou, 1988), normal-mode analysis (Levy and Karplus, 1979; Noguti and Nishikawa, 1983; Levitt et al., 1985) or MD simulations (Levy et al., 1982; Swaminathan et al., 1982; Aqvist et al., 1985; Edholm and Jahnig, 1988; Eriksson et al., 1993). From normal-mode analysis it was found that some of the lowest normal modes, with resonance frequencies of 2–6 cm^{-1}, dominate the overall motions of the protein backbone, i.e., they account for up to 70% of the root-mean-square (rms) fluctuations of the backbone atoms (Levitt et al., 1985). Theoretical considerations (Persson, 1986) and MD simulations (Pleiss and Jahnig, 1991) have shown that immersion of the protein molecule in water drastically changes the nature of the low-frequency modes – the resonance frequency slightly red-shifts and it acquires a large imaginary part, caused by viscous damping.

At present it is assumed that membrane proteins possess a very flexible spatial structure and exhibit strong conformational dynamics on very wide time scales (Popot, 1993), so they are a quite attractive object for exploring their dynamics by NMR. The very complex internal motions were detected by measurements of the ^{15}N NMR relaxation of (1–36)bacterioopsin and (1–71)bacterioopsin polypeptides, comprising the transmembrane α-helix A (sA) or both A and B (C2) of bacterioopsin (Fig. 1) in chloroform–methanol (1:1) and in SDS micelles (Orekhov et al., 1994a,b). After exclusion of the impact of millisecond time scale conformational exchange on ^{15}N amide transverse relaxation rates, the experimental NMR relaxation data were treated in terms of order parameters, as a model-independent measure of the degree of spatial restriction of the internal motions and the effective correlation time of bond motions using the 'model-free' formalism proposed by Lipari and Szabo (1982) and extended by Clore et al. (1990). This approach effectively 'decouples' motions of the different time scales, principally allowing use of the different models to test fast and slow internal motions. In both of the used media, sA and C2 exhibit very similar dynamic properties, closely correlated with their spatial structures (Pervushin and Arseniev, 1992; Pervushin et al., 1994). Generally, the N-H vectors of amide groups were involved in fast thermal fluctuations in the extreme narrowing regime, associated with the order parameters and scarcely depending on the secondary structure of polypeptides, and in more collective intermediate motions on the nanosecond time scale.

As the first step in assessing the mechanics of internal motions of bacterioopsin, in the present paper we develop the dynamic models of one and two transmembrane α-helical peptides based on long (500 ps) MD simulations, along with elastic body representations. In the framework of the models, we consider the impact on the ^{15}N NMR relaxation of the different kinds of internal motions, such as fast thermal fluctuations and elastic deformations of the α-helices.

Models and Methods

Molecular mechanics models for polypeptide spatial structures

For the MD simulations we chose two polypeptides, corresponding to the segment A (residues 1–36) and the two-helical subunit C2 (residues 1–71) of bacterioopsin, whose NMR conformations in methanol–chloroform

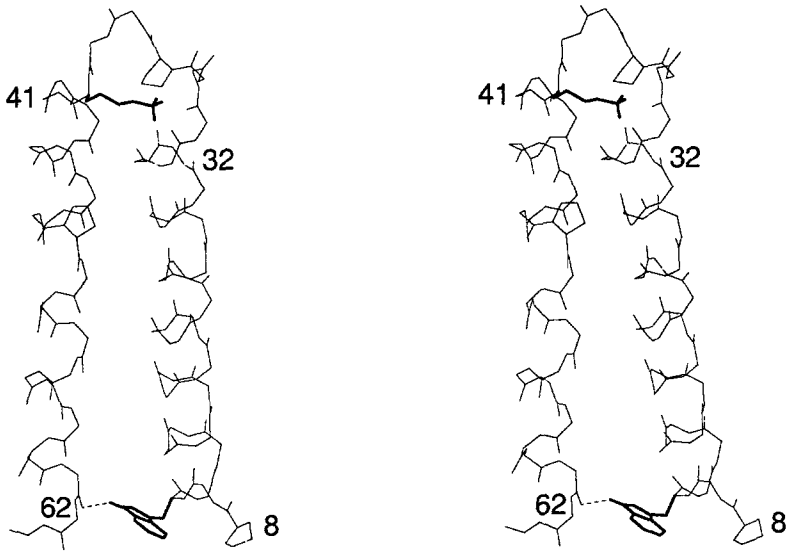

Fig. 1. Stereoview of the conformation of C2, taken at the 100 ps time point of an MD simulation. To ensure the compactness of the structure during MD simulation, the distances between pairs of atoms HZ of Lys^{40} and O of Gly^{31} and HE1 of Trp^{10} and O of Leu^{61} (dashed lines) were constrained. The side chains of Lys^{40} and Trp^{10}, used in the construction of interhelical links, are highlighted. Particular residues are marked by the appropriate numbering.

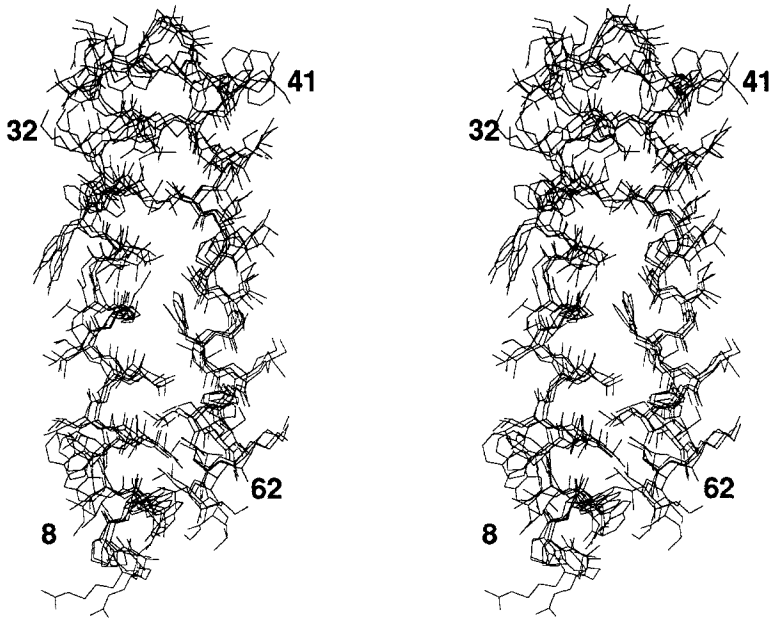

Fig. 2. Stereoview of superpositions of five C2 snapshots, taken at the 10, 100, 200, 300 and 400 ps time points during an MD-simulated trajectory. The positions of residues Pro[8], Met[32], Lys[41] and Gly[63] are marked by the appropriate numbering.

(1:1), 0.1 M $^2HCO_2NH_4$, and sodium dodecylsulfate (SDS) micelles are available from previous investigations (Pervushin and Arseniev, 1992; Pervushin et al., 1994). Because we are interested in modeling the dynamics of the transmembrane α-helices, in the current simulations we omitted the unstructured terminal parts (residues 1–6 and 33–36 for segment A and 1–6 and 64–71 for C2) of the polypeptides with respect to those used in the NMR experiments. For both peptides we retained N-capping of Asn[7] and the subsequent Pro[8], a combination recognized by Richardson and Richardson (1993) to have a strong preference to terminate the N-terminal ends of α-helices in globular proteins. As pointed out by the same researchers, the C-cap position in α-helices is overwhelmingly dominated by glycine residues; Gly[31] and Gly[63] were good candidates for the terminal positions in the model peptides. In the case of sA, we prolonged the α-helix up to Met[32], for in the previous NMR investigation of (1–36)bacterioopsin (Pervushin and Arseniev, 1992), Met[32] was found to terminate the transmembrane α-helix. Pervushin et al. (1994) suggested a closely packed structure of C2 in the organic mixture and in SDS micelles; however, no direct interhelical {^{1}H-^{1}H} NOE was found in NOESY spectra. It is worthwhile to note that in the similar organic mixture of chloroform–methanol–water (4:4:1), Girvin and Fillingame (1994a,b) were able to prove the interaction between the transmembrane α-helices of subunit *c* of F1F0 ATP synthase by ^{1}H NMR investigations of the nitroxide-derivatized subunit *c*. Thus, the MD simulations of C2 were performed with the ends of the transmembrane α-helices being restrained by application of a potential of the form $K*(R_{av}-R)^2$ (with the force constant $K = 100$ kcal/Å^2) to the following pairs of atoms: HZ of Lys[40] and O of Gly[31], and HE1 of Trp[10] and O of Leu[61] (Fig. 1), with average distances $R_{av} = 2.9$ and 2.5 Å, respectively, to ensure the stability of the overall polypeptide structure during the simulation. These restraints were derived from an analysis of the set of NMR conformations of (1–71)bacterioopsin (Pervushin et al., 1994) and were supported by the fact that the lysine side chain can serve as a hydrogen-bond donor and participate in the ionic interactions with the C=O groups of three C-terminal residues of the adjacent α-helix, lacking the corresponding backbone HN counterparts (Fig. 1). As a result of the application of restraints during the MD simulations, no significant violation of the starting NMR structure occurs, as evidenced by the superposition of five C2 'snapshots', taken every 100th ps of the MD time trajectory (Fig. 2), and quite low rmsd values of the heavy atom coordinates throughout the MD trajectory (see Results and Discussion).

Molecular dynamics simulation

In vacuo MD simulations of sA and C2 were carried out using the molecular mechanics program CHARMm (Brooks et al., 1983) on a Silicon Graphics IRIS-220 workstation. All hydrogen atoms were explicitly included. Starting NMR structures were subjected to 1000 steps of energy minimization in a dielectric continuum ($\varepsilon = 10$), followed by 1000 steps of energy minimization with a distance-dependent dielectric permeability ($\varepsilon = r_{ij}$). The minimized structures were heated from 0 to 300 K during 3 ps and equilibrated during 10 ps, with velocities rescaled every 50 steps. The 5 and 500 ps MD runs at 300

K were carried out using the Verlet algorithm with a distance-dependent ε. The nonbonded energies and forces, which were smoothly truncated at 7.5 Å with a shifting function (Brooks et al., 1983), were processed using a list-based algorithm and the list was updated every 10th time step. For the 5 and 500 ps simulations the coordinates and velocities were saved every step (1 fs) and every 100th step (0.1 ps), respectively, and two sets of 5000 'snapshots' each of the atomic coordinates were obtained as output.

Correlation functions, order parameters and effective correlation times

The internal motions of a peptide amide group, resulting in ^{15}N relaxation and ^{1}H-^{15}N cross-relaxation, can be described by the autocorrelation function:

$$C_I(\tau) = \langle r^{-6} \rangle^{-1} \langle P_2[\vec{v}(0) \cdot \vec{v}(\tau)] / [r(0) \cdot r(\tau)]^3 \rangle \quad (1)$$

where $\vec{v}(\tau)$ is the unit vector in the laboratory-referenced coordinate frame directed from the N to the H atom in an amide group, $r(\tau)$ is the N-H distance, $P_2(x) = (3x^2 - 1)/2$ is the second-order Legandre polynomial and the angle brackets indicate the ensemble average. Equation 1 was used to calculate $C_I(\tau)$ from the MD output trajectories. In these cases, ensemble averaging was changed to trajectory averaging. To check the effect on $C_I(\tau)$ of the overall rotation of peptides during the MD simulation, we calculated $C_I(\tau)$ directly from the MD output trajectory and from a new trajectory, generated by determining the rms best-fit superposition of each stored coordinate snapshot with the first coordinate set. No significant difference between thus calculated autocorrelation functions was observed, indicating the absence of significant rotation of peptides during the MD simulation.

The statistical uncertainty resulting from the finite length of the simulated trajectories can be estimated following Zwanzig and Ailawadi (1969):

$$\Delta[C_I(\tau)] = C_I(\tau)[1 - C_I(\tau)](2\tau_e / t_{run})^{0.5} \quad (2)$$

where t_{run} is the trajectory time length, and the ratio t_{run}/τ_e reflects the number of 'events' during this time. In the case of stochastic jumps of the N-H vector, the time τ_e is the correlation time of this process. For the bending motions of the α-helix during MD simulations in vacuo, we qualitatively estimated the statistical uncertainty of $C_I(\tau)$ using Eq. 2, with a characteristic time τ_e on the order of the bending period (about 20 ps). For most of the amide bonds of sA and C2, the uncertainty in $C_I(\tau)$ due to the finite length of the trajectories did not exceed 5% (except in residues 34–39 from the loop region connecting the α-helices A and B of C2, where infrequent jumps between two conformational states were detected).

To compare the theoretical and experimental values of amide ^{15}N relaxation and ^{1}H-^{15}N cross-relaxation rates stipulated by the intramolecular motions, we used the 'model-free' formalism introduced by Lipari and Szabo (1982) and extended by Clore et al. (1990). Available experimental ^{15}N relaxation data are generally insufficient to determine the autocorrelation function explicitly; instead, it is modeled by a simpler function with fewer parameters. Assuming that the overall motion is independent of internal motions, the corresponding autocorrelation function is:

$$C(\tau) = C_I(\tau) \cdot C_R(\tau_R, \tau) \quad (3)$$

where $C_R(\tau_R, \tau)$ is the autocorrelation function of the overall rotation of the molecule and τ_R is the effective correlation time of this rotation. The internal autocorrelation function $C_I(\tau)$ is factorized as:

$$C_I(\tau) = [S_f^2 + (1 - S_f^2)\exp[-\tau/\tau_f]] \cdot [S_s^2 + (1 - S_s^2)\exp[-\tau/\tau_s]] \quad (4)$$

where τ_s is the effective correlation time of internal motions on the intermediate time scale between τ_R and fast thermal fluctuations with correlation time τ_f, and S_f^2 and S_s^2 are the order parameters for motions on the fast and intermediate time scales. Equation 4 was used in the interpretation of ^{15}N relaxation of C2 (Orekhov et al., 1994a) and sA (Orekhov et al., 1994b), both in methanol–chloroform and in SDS micelles. Thus, the order parameters S_f^2 and S_s^2 and correlation times τ_R and τ_s for almost all residues of sA and C2 were obtained.

In the 'model-free' formalism, the order parameters S_i^2 (i = f,s) are interpreted as a model-independent measure of the degree of spatial restriction of the internal motions. S_i^2 ranges from 1 for no internal motion at all to 0 for a completely unrestricted motion. Usually, the generalized order parameter $S^2 = S_f^2 * S_s^2$ and S_f^2 are evaluated by estimating the corresponding plateau value of the autocorrelation function given by Eq. 1 (Palmer and Case, 1992; Eriksson et al., 1993). As was evident from a number of MD simulations (e.g., the zinc-finger peptide xfin31 (Palmer and Case, 1992); BPTI (Swaminathan et al., 1982); and the present calculations), the first plateau is reached at 0.2–0.4 ps. We associated the initial drop of $C_I(\tau)$ with the fast thermal fluctuations of the N-H vector, and related it to the order parameter S_f^2 and correlation time τ_f as:

$$S_f^2 = (0.2 - 0.4)^{-1} \int_{0.2}^{0.4} C_I(\tau) d\tau$$
$$\tau_f = (1 - S_f^2)^{-1} \int_{0.0}^{0.4} [C_I(\tau) - S_f^2] d\tau \quad (5)$$

To obtain a more accurate sampling of the initial values of $C_I(\tau)$ in Eq. 5, the 5 ps MD trajectory was used. The rmsd of the autocorrelation function $C_I(\tau)$ in the integration interval (0.2–0.4 ps) was taken as a simple error estimate of S_f^2.

Due to the negligence of the environment in the MD simulations, most of the low-frequency vibrations of peptides are in the underdamped regime, resulting in almost undecayed harmonic oscillations of the function $C_l(\tau)$ (see Results and Discussion). It thus seems to be quite difficult to obtain a reliable estimate of the generalized order parameter $S^2 = S_f^2 * S_s^2$ using the plateau value of function $C_l(\tau)$ at rather long τ in the limited time trajectories. On the other hand, as was shown by Lipari and Szabo (1982), the generalized order parameter S^2 reflects the spatial restriction of motion and does not depend on the stationary process rate. The order parameter could then be expressed as:

$$S^2 = \sum_{i,j=1}^{N} p(i)\, p(j)\, P_2(\vec{\zeta}_i \cdot \vec{\zeta}_j) \qquad (6)$$

where p(i) is the probability that the unit vector $\vec{\zeta}$ pointing along a particular N-H bond assumes the *i*th orientation, and N is the number of possible discrete orientations. The distribution of this probability is governed only by the relative potential energy surface E_i for the N-H vector (Akke et al., 1993). To derive p(i), the amide nitrogens of each coordinate snapshot were translated to the origin of the laboratory coordinate frame, as the ends of the unit vectors along the amide bond outline the unit sphere surface. Then the sphere was divided into N (128×128) patches with equal area. The vector $\vec{\zeta}_i$ was assigned to be in orientation i if its end fell within the patch number i on the sphere surface. The probability of residency in position i was found to be $p(i) = N_i / \Sigma N_i$, where N_i is the number of vectors that have been cast into patch i, and the summation is over all patches. Generally, for all residues of sA and C2 the values of S^2 calculated using Eq. 6 were smaller than those of S_f^2 calculated by Eq. 5. The error in S^2 calculated by Eq. 6 was estimated from the statistical uncertainties in the determination of p(i). A reliable estimate of p(i) would require the absence in the MD simulations of processes with characteristic times longer than the time length of the MD trajectory. Assuming that the bend vibrations in the underdamping regime with τ_b about 10–50 ps are the longest process exhibited by the α-helix, one could hope to obtain a quite reliable description of p(i), and thence S^2 from the 500 ps MD trajectory. The values of the order parameters of intermediate internal motions, S_s^2, are determined as $S_s^2 = S^2/S_f^2$.

To verify the suggestion that the intermediate motion is stipulated by helix bend vibrations, we calculated S_s^2 using Eq. 6, where $\vec{\zeta}_i$ was substituted for the unit vector $\vec{\mu}_i$ representing the helix axis direction near residue i. To calculate vector $\vec{\mu}_i$, the ideal five-residue α-helix ($\varphi = -57°$ and $\psi = -47°$) with the axis directed to the x-axis of the laboratory coordinate frame (as defined by Chou et al. (1984)) was fitted to the $i-2$ to $i+2$ stretch of the tested α-helix to obtain minimum rmsd values of the corresponding backbone atoms. The vector $\vec{\mu}_i$ was calculated as $\vec{\mu}_i = R \cdot \vec{k}$, where R is the rotational transformation matrix obtained during fitting, and the vector $\vec{k}$ is the unit vector directed along the x-axis.

Elastic rod model

A long transmembrane α-helix immersed in a solvent can be considered as a rod-shaped elastic body in a viscous environment, stochastically vibrating under random forces. Thus, if we assume that amide vectors are rigidly attached to the rod, with the direction almost collinear with the rod axis (see Fig. 4), we can estimate the theoretical values of the order parameters and correlation times of N-H vectors associated with the elastic bend vibrations of the helix. The corresponding eigen-frequencies and the number of excited modes of α-helix oscillations were taken from MD simulations of sA and C2.

Consider an elastic rod of length *l* with the circular cross-section area F, oriented as shown in Fig. 4. The deviation from equilibrium of the rod axis $\mathbf{u}(x,t)$ at point x at time t under random force f is defined as follows (Landau and Lifshitz, 1987):

$$\mathbf{Lu} = f$$
$$\mathbf{L} = \mathbf{EJ}\frac{\partial^4}{\partial x^4} + \rho\mathbf{F}\frac{\partial^2}{\partial t^2} + 2\rho\mathbf{F}\beta\frac{\partial}{\partial t} \qquad (7)$$

where E is the elasticity coefficient, β is the damping parameter, and J and ρ are the momentum and the density of the rod cross section. The random force f is supposed to have a mean value of zero and, in accordance with the fluctuation–dissipation theorem:

$$\langle f(x,t)\, f(x',t') \rangle = \frac{k_B T \cdot 2\beta}{\rho \mathbf{F}} \cdot \delta(x-x')\, \delta(t-t') \qquad (8)$$

where k_B is the Boltzmann constant and T is the temperature. For the autocorrelation function $K_u(x,t,x',t') = \langle \mathbf{u}(x,t)\, \mathbf{u}(x',t') \rangle$ we can write:

$$\underset{x,t}{\mathbf{L}}\ \underset{x',t'}{\mathbf{L}}\, K_u(x,t,x',t') = \langle f(x,t)\, f(x',t') \rangle \qquad (9)$$

For the stationary process, $K_u(x,t,x',t')$ depends only on $\tau = t - t'$ and the autocorrelation function of interest is $K_u(x,x',\tau)$. To solve Eq. 9, the appropriate boundary conditions of $K_u(x,x',\tau)$ are required. If the α-helix constitutes part of a two-helical molecule, we assume that the helix ends are connected by hinge-like junctions at the points $x = 0$ and $x = l$. In that case, the solution of Eq. 9 would be the following (Bolotin, 1978):

$$K_u = \frac{1}{\rho F l} e^{-\beta|\tau|} \sum_{k=1}^{\infty} \frac{1}{\omega_k^2} \left(\cosh \omega_{k\beta}\tau + \frac{\beta}{\omega_{k\beta}} \sinh \omega_{k\beta}\tau \right) \sin\frac{k\pi x}{l} \sin\frac{k\pi x'}{l} \qquad (10)$$

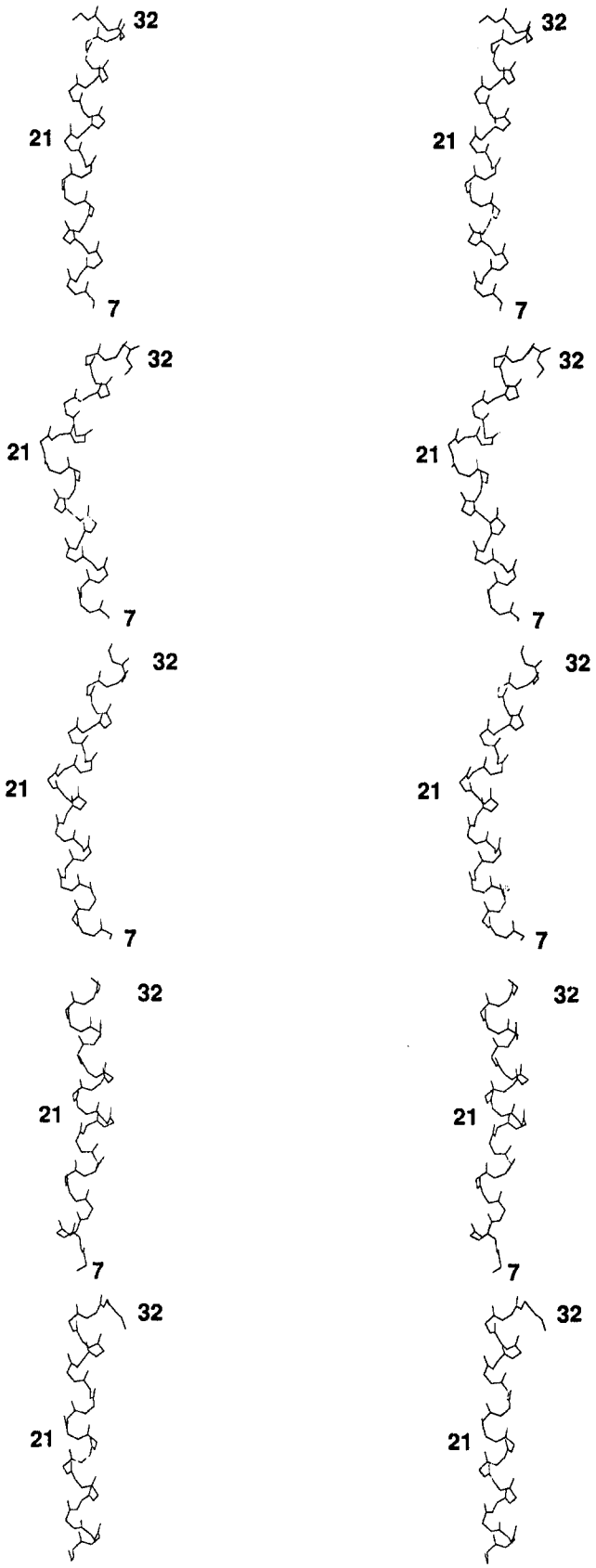

Fig. 3. Stereoviews of the backbone heavy atoms of sA at various time points during an MD simulation (from top to bottom: 10, 100, 200, 300 and 400 ps). The positions of residues Asn^{7}, Gly^{21} and Met^{32} are marked by the appropriate numbering.

where k is the mode number, $\omega_{k\beta}=|\omega_k^2-\beta^2|^{1/2}$, $\omega_k<\beta$ and ω_k is the rod eigen-frequency. In this and the following equations, if $\omega_k>\beta$, then cosh $\omega_{k\beta}\tau$ and sinh $\omega_{k\beta}\tau$ are substituted for cos $\omega_{k\beta}\tau$ and sin $\omega_{k\beta}\tau$, respectively.

For the unit vector $\vec{\mu}(x,\tau)$, directed along the rod axis in a point x at time t (Fig. 4), we have:

$$\vec{\mu}(x,t)=\frac{\vec{n}}{|\vec{n}|}$$
$$\vec{n}=\frac{\partial u_y}{\partial x}\vec{j}+\frac{\partial u_z}{\partial x}\vec{k}+\vec{i} \tag{11}$$

where u_y and u_z are independent ($<u_yu_z>=0$) oscillation modes of bend vibrations in the y- and z-directions represented by unit vectors $\vec{j}$, $\vec{k}$ (vector $\vec{i}$ is directed along the x-axis). The autocorrelation function of the vector $\vec{\mu}(x,\tau)$ in the limit of small amplitudes of oscillations will be as follows:

$$C^b(\tau)=\left\langle P_2[\vec{\mu}(0)\cdot\vec{\mu}(\tau)]\right\rangle\approx\sum_{k=1}^{Q}C_k^b(x,\tau)$$
$$C_k^b(\tau)\approx 1-\left\langle\left(\frac{\partial u_k(0)}{\partial x}\right)^2\right\rangle+\left\langle\frac{\partial u_k(0)}{\partial x}\frac{\partial u_k(\tau)}{\partial x}\right\rangle \tag{12}$$

where $C_k^b(x,\tau)$ is the autocorrelation function for the k-mode of bend vibrations $u_k(x,\tau)$. Index k corresponds to the different frequencies; Q is the number of excited modes at a given temperature. Using Eqs. 10 and 12 one obtains:

$$C_k^b(x,\tau)=1-\frac{2\pi^3RTk^2}{\rho Fl^3\omega_k^2}\cos^2\left(\frac{k\pi x}{l}\right)$$
$$\times\left\{1-e^{-\beta|\tau|}\left(\cosh\omega_{k\beta}\tau+\frac{\beta}{\omega_{k\beta}}\sinh\omega_{k\beta}\tau\right)\right\} \tag{13}$$

Retaining in Eq. 12 only two modes in the y- and z-directions (Fig. 4), corresponding to the first eigen-frequency observed in the MD simulations (see Results and Discussion), the order parameter of the bend vibrations at a point x is estimated as:

$$S_b^2=1-\frac{\pi RT}{Ml^2c^2\nu^2}\cos^2\left(\frac{\pi x}{l}\right) \tag{14}$$

where c is the velocity of light, R is the gas constant, T is the temperature, M is the molar weight of the α-helix and $\nu_1=\omega_1/(2\pi c)$ is the first eigen-frequency of the rod. For the two coupled α-helices of C2 (residues 8–32 and 39–62), M = 2631 and 2658 g/mol, $\nu_1=1.8$ cm^{-1} and 1.6 cm^{-1} (see Results and Discussion), and $l=3.8$ nm for both helices. Thus, the values of order parameter S_b^2 at the ends ($x=0$, $x=l$) are 0.93 and 0.91 for the (8–32) and (39–62) α-helices, respectively, and 1.0 at the center of the α-helices ($x=0.5\,l$).

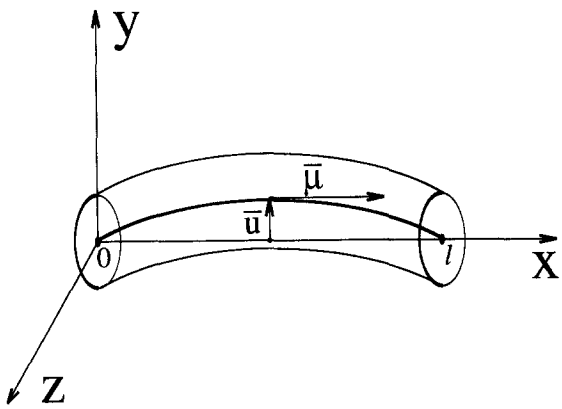

Fig. 4. Elastic rod model of an α-helix of length l. Vector $\bar{u}(x)$ corresponds to the deviation of the axis of the rod from equilibrium at point x. Unit vector $\bar{\mu}(x)$ represents the direction of the axis at point x.

For the single α-helix, free-end boundary conditions should be used to solve Eq. 9. In that case the expression for the order parameters of bend vibrations can easily be shown to have the form:

$$S_b^2 = 1 - \frac{RT}{M\pi^2}\frac{\lambda_n^2}{c^2\nu_l^2}\Gamma_n^2(x)$$

$$\Gamma_n(x) = \frac{(\sinh\lambda_n l - \sin\lambda_n l)}{(\cosh\lambda_n l - \cos\lambda_n l)} \times (\sinh\lambda_n x - \sin\lambda_n x) - (\cosh\lambda_n x + \cos\lambda_n x) \quad (15)$$

and λ_n is the positive root of the equation $\cosh\lambda_n l \cdot \cos\lambda_n l = 1$ (Landau and Lifshitz, 1987). Retaining two modes of vibrations, with the frequency observed in the MD simulation ($\nu_1 = 1.25$ cm^{-1}), and taking $\lambda_1 = 4.73/l$ and M = 2631 g/mol, we obtain an estimation of the order parameter $S_b = 0.85$ at the ends ($x = 0$, $x = l$) and $S_b = 1.0$ in the center of the helix.

Using Eqs. 12 and 13, the correlation time of bending can be calculated for all boundary conditions as:

$$\tau_b = \left(1 - S_b^2\right)^{-1}\int_0^\infty \left[C^b(\tau) - S_b^2\right]d\tau = \frac{2\beta}{\omega_1^2} = \frac{\beta}{2\pi^2 c^2 \nu_1^2} \quad (16)$$

Results and Discussion

MD models of sA and C2

The snapshots of sA and C2 taken every 100th ps during the MD simulation are shown in Figs. 2 and 3, respectively. Parameters of the representative 500 ps time trajectories of sA and C2 are plotted in Fig. 5. Overall, the peptides displayed some deviation from the starting structure; however, for sA distinctive disturbance can be observed, leading to an increase of rms deviations in the time interval 70–160 ps. Close inspection of the corresponding structures reveals a highly localized disruption of the α-helix around Gly^{21}, in which the carbonyl group of Gly^{21} points roughly normal to the helix axis and forms a hydrogen bond with the $H^{\gamma 1}O$ group of Thr^{24}. The structural disturbance is apparent in the backbone representation of the snapshot of the sA structure taken at the 100 ps time point (Fig. 3). The distribution of the orientation of the Gly^{21} N-H vector shows a change in orientation of about 110° (Fig. 6a), while the orientations

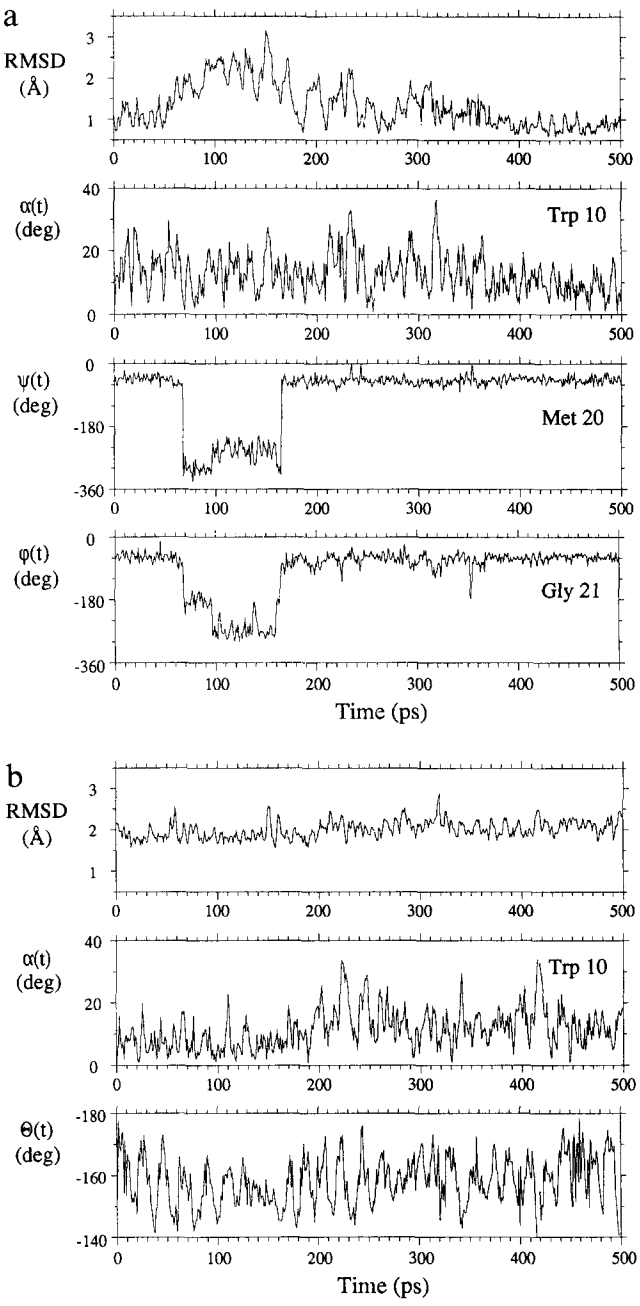

Fig. 5. Time evolution of the rms deviations of backbone coordinates relative to the starting coordinates and the angle $\alpha(t) = \cos^{-1}[\bar{\mu}(0) \cdot \bar{\mu}(t)]$ between the axis of the α-helix $\bar{\mu}_i(t)$ near residue Trp^{10} ($i = 10$) of the starting conformation ($t = 0$) and the conformation at time t of MD simulations of (a) sA and (b) C2. In (a) the evolution of the backbone angles ψ(t) of Met^{20} and φ(t) of Gly^{21} is presented. In (b) the evolution of the tilt angle Θ(t) between the axes of the α-helices A (residues 8–32) and B (residues 40–63) is shown.

of the N-H vectors of the adjacent residues Met[20] and Leu[22] and of other distant residues do not change considerably. Except for ψ of Met[20] and φ of Gly[21] (Fig. 5a), the backbone torsion angles (φ,ψ) of all residues lie near the canonical values (–60°, –40°) throughout the MD simulation. An analogous disturbance of the α-helix was described by Keefe et al. (1993) for a glycine insertion mutant of staphylococcal nuclease and was dubbed α-aneurysm. In contrast to their observation, in our simulation the Gly[21] carbonyl oxygen atom is stabilized not by a hydrogen bond to surrounding water molecules (which are absent in the current simulations), but to the $H^{\gamma 1}O$ group of Thr[24]. A remarkable feature of C2 (Sobol et al., 1992) and of sA (Pervushin and Arseniev, 1992) in methanol–chloroform, 0.1 M $LiClO_4$, was rather slow exchange of the side-chain $H^{\gamma 1}O$ protons of Thr[17], Thr[47], Thr[55], Thr[67] and Ser[59] of C2 and Thr[17] and Thr[24] of sA with solvent. NOESY cross peaks have been found defining the orientations of the side-chain $H^{\gamma 1}O$ groups ($\chi^1 = -60°$) of Thr[17] and Thr[24] to make them optimal for the

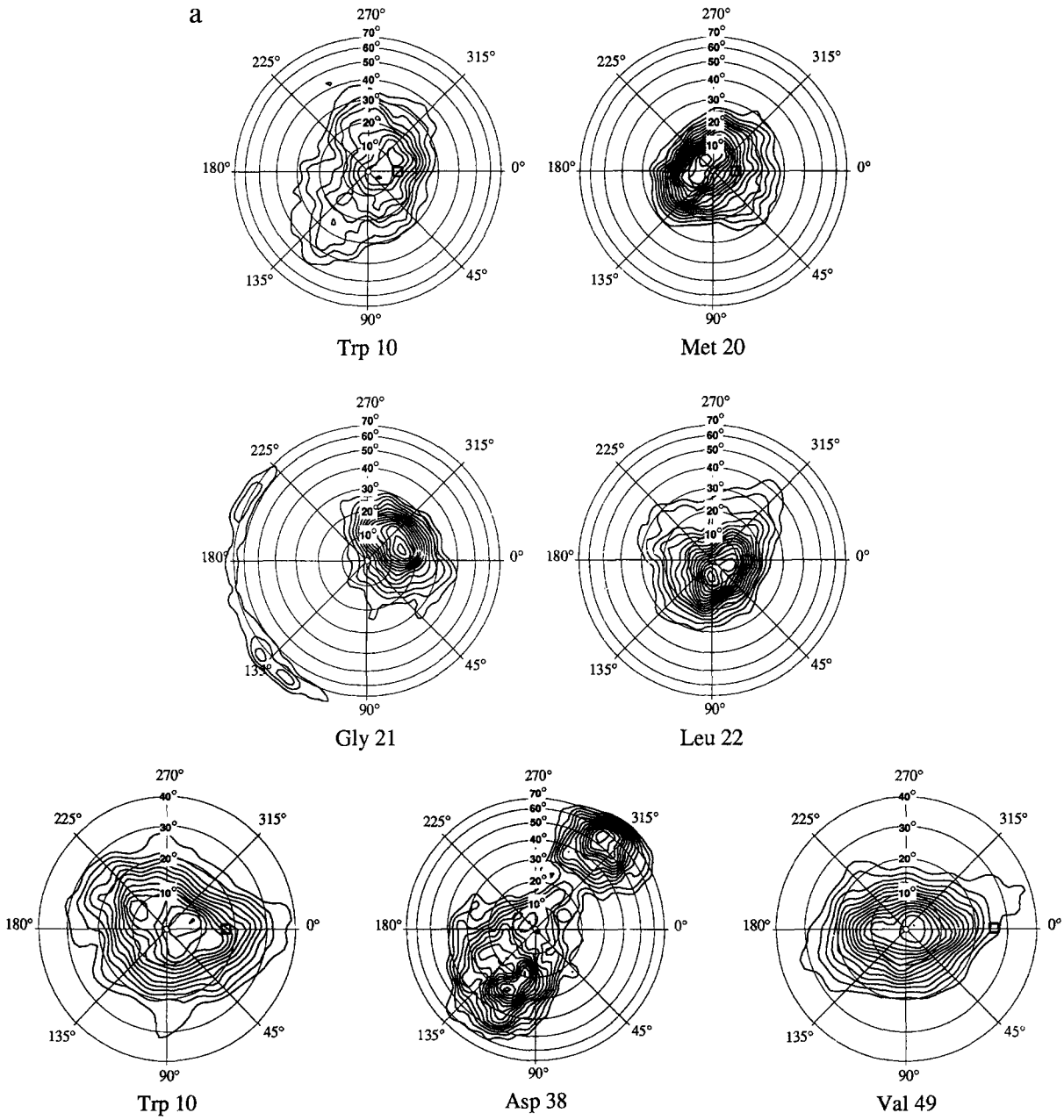

Fig. 6. Probability density maps as a function of polar angles (longitude and latitude) of the orientation of the N-H vector, obtained from the MD simulation of (a) sA (residues 10, 20, 21 and 22) and (b) C2 (residues 10, 38 and 49). The axis of the polar coordinate frame goes through the center of mass of the particular probability distribution. The time trajectory averaged position of the α-helix axis vector near the residue is shown by the black square. The distribution is normalized to have a unit volume. The outmost level corresponds to a 4.25×10^{-2} density of probability to find the NH vector in the unit area on the unit sphere. The increment between contours is 4.25×10^{-2}.

formation of $CO_{i-3,4}$-$H^{\gamma 1}O_i$ hydrogen bonds (Sobol et al., 1992; Pervushin and Arseniev, 1992). Formation of these hydrogen bonds weakens the α-helical backbone hydrogen bonds, due to competition between the $H^{\gamma 1}O$ and HN groups for the C=O group. However, in the MD simulations of both sA and C2 no structural disturbance was found for the Ala^{14}-Thr^{17} region. Analysis of the MD snapshots of sA showed that both a proper orientation of the Thr^{24} side chain and a rather large α-helix bend (more than 30°) are essential to the α-aneurysm distortion. The second condition is much hindered in the closely packed structure of C2. Therefore, no distortion was detected in any of the MD simulations of C2. Because α-aneurysm is a very local disturbance, it scarcely changes the α-helix axis, so the direction of the helix axis calculated near N-terminal residue Trp^{10} was insensitive to the distortion (Fig. 5a).

As can be seen from a trace of torsion angles ψ of Met^{20} and φ of Gly^{21} (Fig. 5a), α-aneurysm occurs for quite a long time (90 ps, i.e., 18% of the total simulation time). From the 500 ps simulation it is impossible to estimate the exchange rate k_{ex} between the classical α-helix and the disturbed one. On the other hand, depending on k_{ex}, such a very local exchange process would lead to the relative decrease or increase of the transverse magnetization relaxation rate (R_{Sx}) of the amide nitrogen of Gly^{21}. If $k_{ex} > 1/\tau_R$, this exchange would decrease R_{Sx}, so it would be reflected by the experimental order parameters of the internal motion. If k_{ex} is in the range 0.1 s^{-1}–1 μs^{-1}, one could expect R_{Sx} to be increased due to the chemical exchange line broadening. Indeed, for sA in methanol–chloroform the relaxation rate R_{Sx} of the amide ^{15}N of Gly^{21} was found to be 7.1 ± 0.5 s^{-1}, thus distinctively exceeding average relaxation rates of 5.7 ± 0.2 s^{-1} for residues in the α-helix (Orekhov et al., 1994b). Based on this observation and on the fact that the measured ^{15}N transverse relaxation rate of Gly^{21} did not depend on the used spin-lock CPMG pulse-train repetition rates, the k_{ex} is estimated to be within the range 1 ms^{-1}–1 μs^{-1}. Thus, this process was excluded from the calculation of the order parameters of internal motion on the nanosecond time scale, and the corresponding autocorrelation functions were calculated starting from the 180 ps time point.

The overall spatial structure of C2 remained almost intact throughout the MD simulation (Fig. 2). A short unrestrained MD run of C2 showed that two restraints used to model the electrostatic interactions at the ends of the coupled α-helices are essential to ensure the stable and closely packed structure of C2. On the other hand, these links induced an additional type of internal motion in C2, connected with a change of the tilt angle between the axes of the coupled α-helices (Fig. 5b). For residues Ser^{35}-Ala^{39}, constituting the loop region between the α-helices A and B, several conformational states were found which led to significant changes in the orientations of the

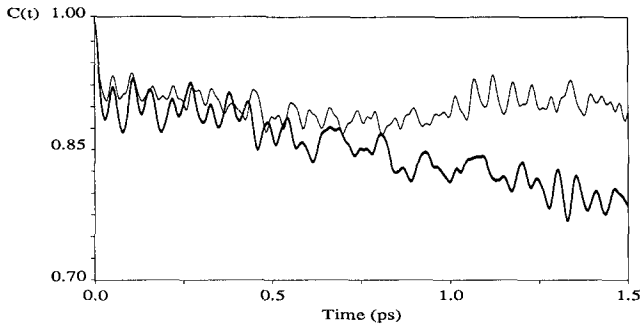

Fig. 7. Short-time autocorrelation functions for the NH vectors of Trp^{10} (bold line) and Val^{49} (thin line), obtained from an MD simulation of C2. Calculations were made using 5000 snapshots of C2 conformations, sampled each femtosecond of the MD time trajectory.

N-H vectors (a representative example, Asp^{38}, is shown in Fig. 6b). Analyses of the snapshots of C2 showed that the N-H vectors of the loop residues exhibited 3–8 jumps between a few relatively stable orientations during the 500 ps MD-simulated time trajectory. As for Gly^{21} of sA, such a process may lead to an increase or decrease of R_{Sx} of the corresponding nitrogens. Because for the loop residues of C2 distinctive decreases in R_{Sx} were observed in the ^{15}N NMR relaxation measurements, both in organic mixture and in SDS micelles (Fig. 4 in Orekhov et al., 1994a), we estimated the k_{ex} of such infrequent jumps to be larger than $1/\tau_R \approx 10^8$ s^{-1}. Due to the fact that the 500 ps MD simulation scarcely samples those events, the order parameters for the intermediate time-scale motions in the loop region of C2 were determined with very large uncertainties, and should be considered only qualitatively.

Autocorrelation functions of internal motions

The shapes of the autocorrelation functions $C_l(\tau)$ for internal motions of N-H vectors calculated by Eq. 1 were similar for all residues constituting the α-helical stretches of both peptides (Figs. 7–9). Generally, rapid initial decays (< 1.0 ps), followed by a plateau superimposed with almost undamped oscillations were observed. In a few cases, for residues in the N- and C-termini of the α-helices and in the loop (residues 34–39) connecting two α-helices in C2, the plateau extends for a shorter time (< 10–40 ps) and $C_l(\tau)$ decays again (Fig. 8). The behavior of the autocorrelation functions implicates several types of internal motions exhibited by the N-H vectors in the peptides. The fastest motions are high-frequency oscillations (200–800 cm^{-1}) of small magnitude, while the others have a more collective nature, considerably lower frequency and a larger amplitude. The high-frequency oscillations are local and correspond to the librational motions of the individual N-H vectors in an effective potential. As pointed out by Swaminathan et al. (1982), this potential is a summation of dihedral angle terms and of nonbonded interactions with the surrounding protein matrix atoms. The high-frequency oscillations, which are present for all

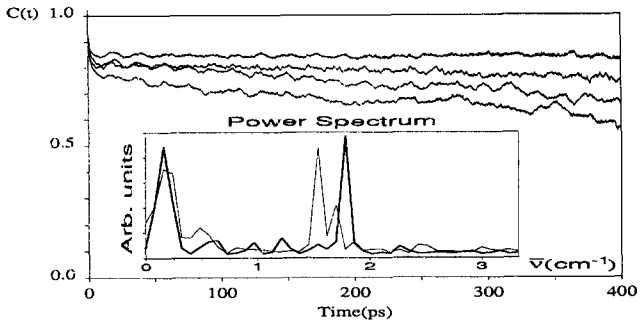

Fig. 8. Autocorrelation functions for the N-H vectors of (from top to bottom) Val[49], Leu[61], Trp[10] and Val[34]. The low-frequency part of the power spectrum of the autocorrelation functions of Trp[10] (thin line) and Val[49] (bold line) is shown in the inset. Before Fourier transformation, a linear baseline correction of the autocorrelation function was made to remove the strong peak at zero frequency. Calculations were made using 5000 C2 snapshots, sampled each 0.1 ps of the MD time trajectory.

N-H vectors, are irregular in character, due to perturbations of the librational motion by collisions with neighboring atoms. This results in the rapid initial decay distinctively observed in the autocorrelation functions of all N-H vectors (Figs. 7 and 8). The order parameters S_f^2 for such motions, determined by Eq. 5, fall within the range 0.85–0.94 and correlation times are about 40–100 fs and independent of the secondary structure (Fig. 10a,b). The calculation of the order parameters S_f^2 from the probability distribution (Eq. 7) of preliminary superimposed α-helix fragments comprising 5–7 residues, to eliminate the collective motion contribution, gave essentially the same results for S_f^2 (data not shown).

Oscillating waves and gentle slopes on the autocorrelation functions are connected with more collective motions of the N-H vectors, on a slower time scale. These oscillations cause the distinct peaks around 1.2–1.8 cm^{-1} in the power spectra of the autocorrelation functions shown in the insets of Figs. 8 and 9. Spurious wraps around zero frequency are remnants of the elimination of a very broad peak, stemming from the fast initial decay of the autocorrelation functions. Oscillations usually originate from harmonic-like deformations of the helix, like stretch and bend vibrations (Chou et al., 1984). Oscillations can be seen from the time traces of the α-helix axis vectors $\vec{\mu}_i$ of C2 and sA, represented in Figs. 5a and b for Trp[10]. The corresponding autocorrelation functions of the vectors $\vec{\mu}_i$ shown in Fig. 9 clearly reflect almost undecayed oscillations. The continuously decaying autocorrelation functions of the N-H vectors correspond to 'slow' motions, like infrequent jumps of the amide bond between several preferred orientations. Such motions could be found for residues from the terminal and loop regions of C2 and for the Gly[21] α-aneurysm of sA (see above). Reliable estimates of the order parameters and correlation times of such rare events would require considerably (> 10–100 times) longer MD simulation runs.

Collective motions of α-helices

The collective motions of the α-helices should be associated mainly with the bending and stretching processes, previously well characterized for the poly-alanine α-helix using MD simulations (Pleiss and Jahnig, 1991). The stretch vibrations have only little impact on ^{15}N NMR relaxation, because they do not significantly change the orientations of the N-H vectors. This is supported by the observation that in the power spectrum of the N-H vector autocorrelation functions, defined as in Eq. 1, only peaks with frequencies corresponding to bend vibrations were found. Graphical inspection of the helices reveals that the bend extends more or less homogeneously along the helix (Figs. 2 and 4). The bending amplitudes are similar for both helices, i.e., on average 20° (Figs. 5a,b). To analyze the influence of the bend vibrations on ^{15}N NMR relaxation, the autocorrelation functions of vector $\vec{\mu}_i$, representing the direction of the α-helix axis near residue i, were calculated by Eq. 1, where r(t) was held constant at 1. Figure 9 shows the autocorrelation function of the bend angle, exhibiting almost undamped oscillations. The power spectrum of this function (inset Fig. 9) contains the highest frequencies at 1.8 cm^{-1}. As there are no peaks in the power spectra at higher frequencies, the procedure for the elucidation of vector $\vec{\mu}_i$ effectively eliminates the influence of the other types of vibration. The NMR relaxation of ^{15}N nuclei is governed both by the order parameter S_s^2 and the correlation time τ_s (see Eq. 4). Thus, it is instructive to elucidate both, in order to answer the question of how much the α-helix bend vibrations contribute to NMR relaxation.

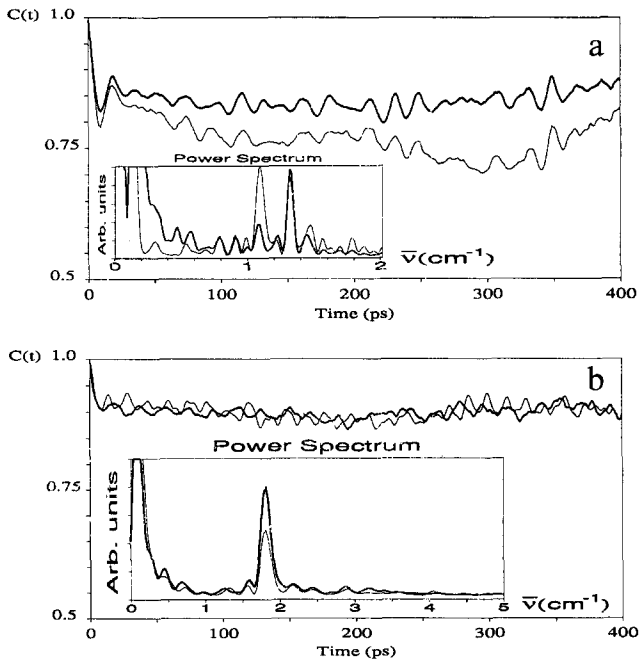

Fig. 9. Autocorrelation functions of unit vector $\vec{\mu}_i$ directed along the α-helix axis near residue i for (a) sA, Trp[12] (bold line) and Thr[24] (thin line), and (b) C2, Trp[12] (bold line) and Ile[58] (thin line). The power spectrum was obtained as described in the legend to Fig. 7.

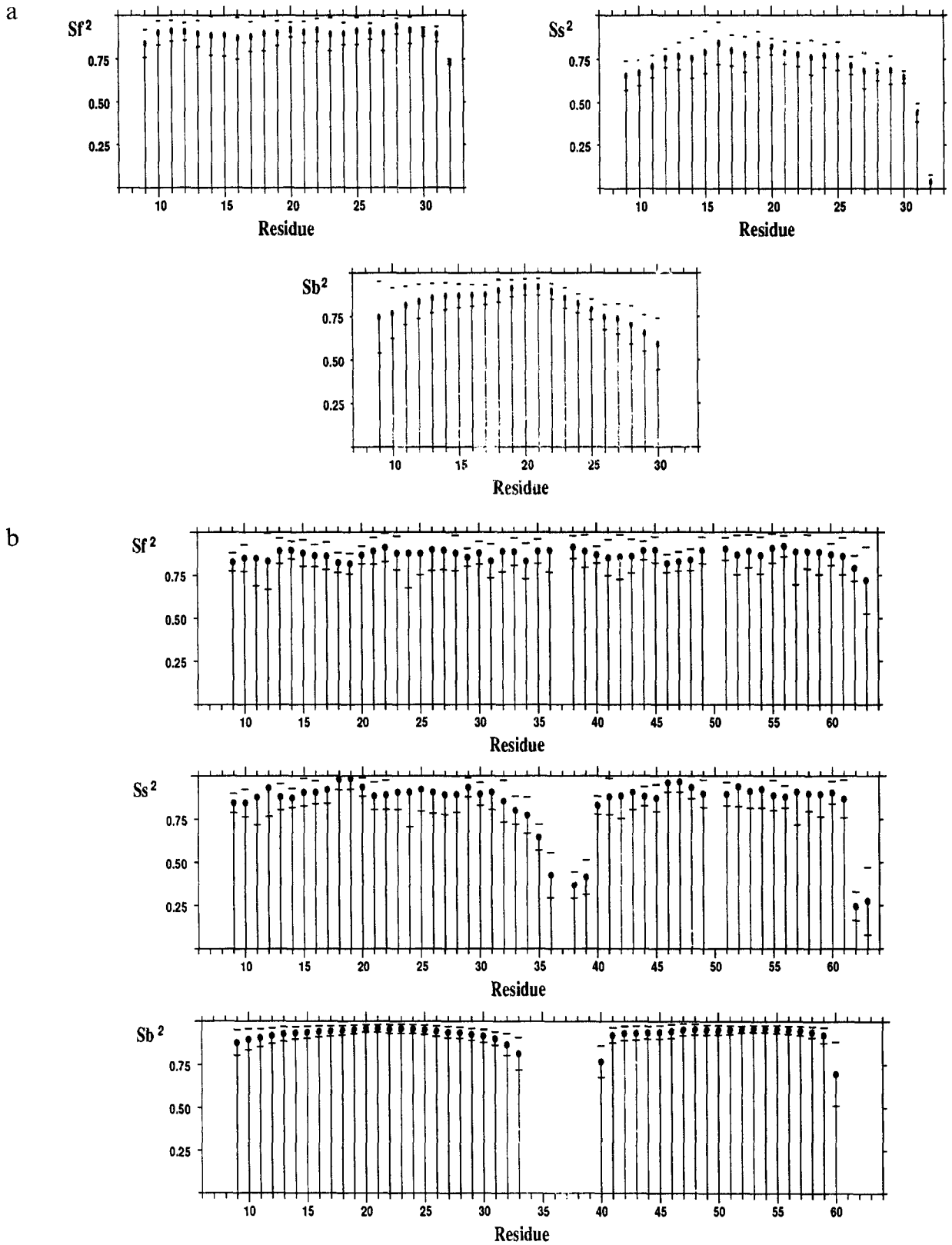

Fig. 10. Order parameters S_f^2 of fast fluctuations of N-H vectors, S_s^2 of all motions of N-H vectors on the nanosecond time scale and S_b^2 of bend vibrations of (a) sA and (b) C2. The error bars indicate uncertainties, estimated as described in the text.

Order parameters of internal motions

The order parameters obtained from the MD simulations, i.e., S_f^2 of the fast thermal librations of the N-H vectors, S_s^2 of motions on the nanosecond time scale and S_b^2 of the bending of the α-helix axis, are presented in Fig. 10. In contrast to S_f^2, the order parameters S_s^2 and S_b^2 are

sensitive to secondary structure. In the α-helical stretches of sA and C2, the parameters S_s^2 and S_b^2 have the characteristic cosine-type envelope approaching a unit value at the center of the α-helix, as was predicted by the elastic rod model (Eqs. 14 and 15). For sA, the S_b^2 are systematically lower than for C2, which is also in close agreement with Eqs. 14 and 15. Comparison of S_s^2 and S_b^2 for both peptides (Fig. 10) leads to the conclusion that bend vibration contributes up to 85–95% of the order parameters S_s^2 of the helix internal motions. This implies the existence of an additional molecular mechanism of delocalized internal motions, slightly contributing to S_s^2. For C2, one of the possible mechanisms is oscillation of the tilt angle between the coupled α-helices (Fig. 5b), with a characteristic frequency comparable to that of bend vibrations of the single α-helix and with an order parameter $S_t^2 = 0.89 \pm 0.03$, as calculated by Eq. 6.

During the MD simulation of sA, the C-terminal residues Gly^{31} and Met^{32} exhibited infrequent jumps between several conformations, resulting in a significant decrease of the order parameters S_s^2 and S_f^2 (for Met^{32}; Fig. 10a). In C2 these residues retained the α-helical conformation, as reflected by the considerably higher values of S_s^2 (Fig. 10b). It should be noted that during the MD simulation, the C-terminal residues Leu^{62} and Gly^{63} of C2 also adopt several conformations that contradict the NMR data (Pervushin et al., 1994). These spurious effects might be caused by the truncation of the amino acid sequences of sA and C2 in the MD simulations, and the corresponding two C-terminal residues have to be ruled out from comparison with the experimental ^{15}N NMR parameters.

MD studies of the proline-containing α-helix F of bacterioopsin (Sankararamakrishnan and Vishveshwara, 1993) showed that Pro^{86} significantly changes the geometrical features of the α-helix and imparts additional flexibility to it. However, as these α-helix distortions are quite local, Pro^{50}, situated in the center of α-helix B of C2, did not have a significant effect on the order parameters of the amide bonds of adjacent residues (Fig. 10). The averaged values of S_s^2 for the first and second α-helices of C2 are identical within experimental error. However, comparing these values with the S_s^2 of residues Ala^{18}, Leu^{19} and Met^{20}, located in the center of α-helix A, a small relative drop of the order parameters S_s^2 for residues Val^{49} and Ala^{51}, adjacent to Pro^{50}, is observed. The order parameters S_b^2 of the bend motions of α-helix B are insensitive to the presence of Pro^{50} (Fig. 10b). The experimental NMR observations also did not reveal an essential effect of Pro^{50} on the order parameters S_s^2 in α-helix B (Orekhov et al., 1994a).

Damping of bend vibrations and relaxation times

For a correct estimation of the correlation times τ_s of motions on the nanosecond time scale, an MD simulation of several nanoseconds is required for solvated peptides, which is still a challenge for currently available computers and calculation methods. However, the correlation time τ_b of bend vibrations is determined by the damping parameter of the environment, as well as by the eigen-frequencies of the vibrations, in accordance to Eq. 16. Previously (Pleiss and Jahnig, 1991), the effect of environment on α-helix dynamics was studied by coupling the helix to a heat bath (none, weak or strong coupling regime) or to water. It was concluded that the eigen-frequencies of the stretch and bend vibrations of the helix are determined essentially by the interactions among helix atoms, whereas the coupling to the environment determines damping. The presence of ambient water slightly increases the stretch vibration damping compared to the case of weak coupling to a heat bath, but the vibration remains underdamped with $\beta \approx \omega_l$. This implies that stretch vibrations hardly contribute to ^{15}N NMR relaxation, due to the fact that their frequencies remain far from the frequencies of nuclear transitions. In contrast, a water environment considerably increases damping of the bend vibration ($\beta \approx 100\ \omega_l$) (Pleiss and Jahnig, 1991). The bend vibrations become overdamped, i.e., their dynamic behavior changes from oscillation to relaxation. Instead of trying more or less correctly to simulate the molecular dynamics of sA or C2 in the environment of SDS micelles or an organic solvent mixture with salt, we used MD simulations in vacuo to retain underdamped or scarcely damped bend vibrations, in order to circumvent the problem of a statistically reliable description of bending motions during the MD trajectory.

As can be seen from Eq. 16, the damping parameter β is crucial to obtain correlation times τ_b of the internal motions on the intermediate time scale that are comparable with the NMR experimental ones. Thus, if the bend vibration correlation time $\tau_b = \tau_s \approx 0.8$ ns (NMR experiments; Orekhov et al., 1994a,b), from Eq. 16 we obtain an estimation of the damping factor $\beta \approx 4 \times 10^{15}\ \text{rad} \times \text{s}^{-1}$, and $\beta/\omega_l \approx 100$, which agrees well with results obtained in MD simulations of the water-solvated 20-residue polyalanine α-helix (Pleiss and Jahnig, 1991).

Comparison of calculated order parameters with experimental results

From ^{15}N NMR relaxation experiments, the order parameters S_f^2 of internal fast motions in the extreme narrowing regime and S_s^2 of motions with correlation times $\tau_s = 0.8 \pm 0.3$ ns for sA and C2 in organic solvent and in micelles are available (Orekhov et al., 1994a,b). A comparison between the NMR experimental and the MD simulation-derived order parameters of internal motions of sA and C2 showed a good fit. Within experimental error, the MD simulation excellently reproduces the order parameters S_f^2 of fast thermal fluctuations of the N-H vectors. The correlation times $\tau_f = 40$–100 fs are well below the fast limit (20 ps), so that the NMR magnetic field provides an extreme narrowing regime for these

motions. The MD-derived order parameters S_s^2 of intermediate motions, however, could not be compared directly to NMR data. The reason for this is that the parameters S_s^2 are coupled with τ_R when Eq. 4 is used in the 'model-free' evaluation of ^{15}N relaxation, and they could not be obtained separately based on ^{15}N relaxation measurements only (Orekhov et al., 1994b). However, the experimental order parameters S_s^2 have a characteristic cosine-type shape in the α-helical stretches and decrease significantly in the unstructured terminal regions (residues 1–7 and 31–36 for sA and 1–7 and 64–71 for C2) and in the loop region (residues 33–41) of C2.

Conclusions

It has been suggested long ago (Lipari et al., 1982) that MD simulation is a powerful tool which could provide a comprehensive model, resulting in realistic order parameters and correlation times for the internal motions in proteins. As long as the internal motions of proteins occur in the extreme narrowing time limit, MD simulations seem to provide an adequate basis for the interpretation of NMR relaxation. As has been shown (Swaminathan et al., 1982), fast internal motions usually are weakly coupled to the environment, so the adequate modeling of the latter is not a bottleneck for the correct representation of these motions. In contrast, internal motions on the nanosecond time scale imply concerted collective vibrations of a large number of atoms, which could be superimposed on the local stochastic distortions of the secondary structure. Owing to their relatively low eigen-frequencies (<2 cm^{-1}), these vibrations are well excited at 300 K and have significant amplitudes (about 3 Å at the ends of the single α-helix). Obviously, this kind of motion is strongly affected by the environment, which effectively overdamps the vibrations from oscillation to relaxation. To explore these motions, one needs a relatively long (longer than the relaxation times of the collective motions) MD simulation, as a rule, with coupling to the environment.

An alternative approach is to use a combination of MD simulations with more simple mechanic models which could be treated theoretically. Assuming that the fast and nanosecond time-scale internal motions are statistically independent, we used MD simulations to assay the fast internal motions and a mechanic model of an elastic rod under stochastic violation, representing the α-helix, to test the bending motions. Within the framework of this combined model, we interpreted the numerical values of the experimental order parameters of fast motions S_f^2, which we concluded to be in the extreme narrowing time limit, and S_s^2 of α-helix collective motions with correlation times τ_s on the nanosecond time scale. The α-helix bend vibration as an elastic rod-shaped body contributes for the major part to the order parameters of the nanosecond time-scale motion of the N-H vectors, thus governing ^{15}N NMR relaxation. A few other molecular mechanisms, such as local distortions of the α-helix (e.g., α-aneurysm) or delocalized α-helical backbone distortions, could also contribute to the experimentally observed dynamic parameters of the internal motions.

Comparison of the sA and C2 MD simulations showed that interactions between the adjacent α-helices could lead to additional internal vibrational degrees of freedom, connected with changes in the orientation of the helices relative to each other, which can also influence NMR relaxation. As pointed out by Chou (1988), these additional vibrational degrees of freedom may significantly contribute to the free energy of the α-helix association process, provided the frequencies are relatively low. For example, if one of the generated vibrational degrees of freedom has a vibration frequency of 1.2 cm^{-1}, then it will contribute an entropy of $\Delta S \approx 12$ eu, which corresponds to a free energy of $\Delta G = -T\Delta S \approx -3.6$ kcal/mol under physiological conditions. Considering that usually several degrees of freedom are generated (Chou, 1988), one obtains an energy term comparable to the contribution from hydrophobic interactions (Sharp et al., 1991). Clearly, such vibrational motions have to be accounted for in construction of thermodynamic models of functioning proteins. Recently Akke et al. (1993) showed that NMR order parameters might serve as a measure of the entropic free energy term in thermodynamic calculations of the cooperative binding of Ca^{2+} by calbindin D_{9k}. In the current investigation, we were limited by the quite far-fetched model of interaction of the α-helices in C2, thus only qualitative conclusions and surmises are valid. If a dynamic model of membrane proteins would be developed, NMR relaxation measurements might become a unique technique in assaying their thermodynamic properties.

Acknowledgements

This research is supported by Grant MIP000 from the International Science Foundation.

References

Akke, M., Bruschweiler, R. and Palmer III, A.G. (1993) *J. Am. Chem. Soc.*, **115**, 9832–9833.

Aqvist, J., Van Gusteren, F.W., Leijonmarck, M. and Tapia, O. (1985) *J. Mol. Biol.*, **183**, 461–477.

Barchi, J.J., Grasberger, B., Gronenborn, A.M. and Clore, G.M. (1994) *Protein Sci.*, **3**, 15–21.

Bolotin, V.V. (1978) *The vibrations in the Machines*, Vol. 1, Machinostroenie, Moscow, pp. 310–318.

Brooks, B.R., Bruccoleri, R.E., Olafson, B.D., States, D.J., Swaminathan, S. and Karplus, M. (1983) *J. Comput. Chem.*, **4**, 187–217.

Bruschweiler, R., Roux, B., Blackledge, M., Griesinger, C., Karplus, M. and Ernst, R.R. (1992) *J. Am. Chem. Soc.*, **114**, 2289–2302.

Chou, K.C., Nemethy, G. and Scheraga, H.A. (1984) *J. Am. Chem. Soc.*, **106**, 3161–3170.

Chou, K.C. (1988) *Biophys. Chem.*, **30**, 3–48.
Clore, G.M., Szabo, A., Bax, A., Kay, L.E., Driscoll, P.C. and Gronenborn, A.M. (1990) *J. Am. Chem. Soc.*, **112**, 4989–4991.
Edholm, O. and Jahnig, F. (1988) *Biophys. Chem.*, **30**, 279–292.
Eriksson, M.A.L., Berglund, H., Hard, T. and Nilsson, L. (1993) *Proteins*, **17**, 375–390.
Girvin, M.E. and Fillingame, R.H. (1994a) *Biochemistry*, **32**, 12167–12177.
Girvin, M.E. and Fillingame, R.H. (1994b) *Biochemistry*, **33**, 665–674.
Keefe, L.J., Sondek, J., Shortle, D. and Lattman, E.E. (1993) *Proc. Natl. Acad. Sci. USA*, **90**, 3275–3279.
Landau, L.D. and Lifshitz, E.M. (1987) *Theoretical Physics*, Vol. 7, Nauka, Moscow, pp. 109–119.
Levitt, M., Sander, C. and Stern, P.S. (1985) *J. Mol. Biol.*, **181**, 423–436.
Levy, R.M. and Karplus, M. (1979) *Biopolymers*, **18**, 2465–2495.
Levy, R.M., Perahia, D. and Karplus, M. (1982) *Proc. Natl. Acad. Sci. USA*, **79**, 1346–1350.
Lipari, G. and Szabo, A. (1982) *J. Am. Chem. Soc.*, **104**, 4546–4559.
Lipari, G., Szabo, A. and Levy, R.M. (1982) *Nature*, **300**, 197–198.
Noguti, G.N.T. and Nishikawa, T. (1983) *Proc. Natl. Acad. Sci. USA*, **80**, 3669–3700.
Orekhov, V.Yu., Pervushin, K.V. and Arseniev, A.S. (1994a) *Eur. J. Biochem.*, **219**, 887–896.
Orekhov, V.Yu., Pervushin, K.V., Korzhnev, D.M. and Arseniev, A.S. (1994b) manuscript in preparation.
Palmer III, A.G. and Case, D.A. (1992) *J. Am. Chem. Soc.*, **114**, 9059–9067.
Persson, B.N.J. (1986) *Chem. Phys. Lett.*, **127**, 428–431.
Pervushin, K.V. and Arseniev, A.S. (1992) *FEBS Lett.*, **308**, 190–196.
Pervushin, K.V., Orekhov, V.Yu., Popov, A., Musina, L.Yu. and Arseniev, A.S. (1994) *Eur. J. Biochem.*, **219**, 571–583.
Pleiss, J. and Jahnig, F. (1991) *Biophys. J.*, **59**, 795–804.
Popot, J.L. (1993) *Curr. Opin. Struct. Biol.*, **3**, 532–540.
Richardson, J.S. and Richardson, D.C. (1993) *Science*, **240**, 1648–1652.
Sankararamakrishnan, R. and Vishveshwara, S. (1993) *Proteins*, **15**, 26–41.
Sharp, K.A., Nicholls, A., Friedman, R. and Honig, B. (1991) *Biochemistry*, **30**, 9686–9697.
Sobol, A.G., Arseniev, A.S., Abdulaeva, G.V., Musina, L.Yu. and Bystrov, V.F. (1992) *J. Biomol. NMR*, **2**, 161–171.
Swaminathan, S., Ichiye, T., Van Gusteren, F.W. and Karplus, M. (1982) *Biochemistry*, **21**, 5230–5241.
Szyperski, T., Luginbuhl, P., Otting, G., Güntert, P. and Wüthrich, K. (1993) *J. Biomol. NMR*, **3**, 151–164.
Wagner, G. (1993) *Curr. Opin. Struct. Biol.*, **3**, 748–754.
Zwanzig, R. and Ailawadi, N.K. (1969) *Phys. Rev.*, **182**, 280–283.